



HAL
open science

Complex evaporation kinetics of a volatile droplet of methanol

A. Dourari, R. Lankri, S. Chikh, S. Khalfallah, Lounès Tadríst

► **To cite this version:**

A. Dourari, R. Lankri, S. Chikh, S. Khalfallah, Lounès Tadríst. Complex evaporation kinetics of a volatile droplet of methanol. *International Communications in Heat and Mass Transfer*, 2023, 144, pp.106741. 10.1016/j.icheatmasstransfer.2023.106741 . hal-04065470

HAL Id: hal-04065470

<https://hal.science/hal-04065470v1>

Submitted on 11 Apr 2023

HAL is a multi-disciplinary open access archive for the deposit and dissemination of scientific research documents, whether they are published or not. The documents may come from teaching and research institutions in France or abroad, or from public or private research centers.

L'archive ouverte pluridisciplinaire **HAL**, est destinée au dépôt et à la diffusion de documents scientifiques de niveau recherche, publiés ou non, émanant des établissements d'enseignement et de recherche français ou étrangers, des laboratoires publics ou privés.

Complex evaporation kinetics of a volatile droplet of methanol

A. DOURARI¹, R. LANKRI¹, S. CHIKH², S. KHALFALLAH¹, L. TADRIST³

¹ Ecole Militaire Polytechnique, Bordj El Bahri, 16046 Alger, Algeria

² USTHB, Faculty of Mechanical and Process Engineering, LTPMP, 16111 Alger, Algeria

³ Aix Marseille Université, CNRS, Laboratoire IUSTI, UMR 7343, 13453 Marseille, France

Abstract

An experimental study is carried out to investigate the different stages of the evaporation phenomenon of a methanol drop that exhibits a complex behavior because of its high volatility. An optical technique is employed with top and side view cameras; it allows to follow the drop shape evolution and determine the geometric parameters: contact angle and base diameter from which the volume of the droplet is computed. The outcomes of this study show three distinct stages. First, the evaporation kinetics is very fast (33% of the droplet lifetime) where 85% of the volume evaporates with a nearly pinned contact line. It is followed by a short stage (12% of lifetime) where 8% of the volume evaporates. In this stage, the drop forms a thin liquid film followed by a motion of the contact line in which the drop retracts. The wetting surface deforms and loses its quasi-circular shape. Then, the wetting area shrinks drastically to form a smaller droplet with a higher contact angle. In the third stage (55% of lifetime), the 7% remaining drop volume evaporates with a low evaporation rate accompanied by a strong decrease of contact angle and a slight decline of wetting area until total evaporation.

Keywords: sessile drop, methanol evaporation, high liquid volatility, wetting area, retraction

1. Introduction

The evaporation of a sessile drop has been the research subject of increasing interest over the last two decades. It is encountered in several industrial and biological applications such

as combustion [1], spray cooling [2], printing technologies [3], DNA mapping [4], self-cleaning surfaces [5], manufacturing of new electronic and optical devices [6], biodiagnostics, medical testing and others [7]. The numerous investigations have led to a significant improvement in the understanding and description of the phenomenon. Particular emphasis has been placed on the problems of wettability and drop shape during evaporation and the interaction between these two phenomena. The pioneer works of Laplace [8] and Young [9] have remained the basis of contemporary research on surface phenomena. More recently, the evolution of microscopic observation techniques has led to an explosion in the number of publications in recent years [10-12]. Depending on the surface properties, different evaporation modes have been observed and explored: the constant angle evaporation mode, for which the contact area between the drop and the substrate decreases, the constant contact-area evaporation mode, for which the contact angle decreases and the combination of these two modes (Stick-Slip mode) [13-15]. Despite the large number of works in the field of sessile drop evaporation, many questions remain unanswered. The majority of the work done in the literature on drop evaporation concerns the evaporation of water [16-17]. There is a limited number of works concerning other liquids, in particular the case of fluids with a higher volatility than water [18-20]. Most of the studies that dealt with alcohol, focused on ethanol-water binary mixtures. To our best knowledge, there is very little work done on either methanol-water mixture droplets or pure methanol droplets maybe due to its high toxicity. It can be said that the previous works were concerned with water-methanol mixtures [21-23] and only few studies dealt with pure methanol [24-28]. The latter focused on the evaporation mechanism of the drop in an incomplete way. The transition phase is just mentioned without being analysed [24,26] or was not reported at all [25,27,28] due to the limitation of visualization because they used a single front camera. We found no results in the literature that could be compared with because of different operating conditions and substrate nature.

As a result, the transition phase is still an open question and more investigations are needed for better understanding of the phenomena. We aim to present our experimental results to allow an in-depth insight of the evaporation dynamics of pure methanol droplets including the transition phenomena.

The objective of this study is to analyze the behavior of a methanol drop and its evaporation kinetics. An optical experimental technique is used during the different tests. It is based on monitoring the geometry of the drop by video imaging, which is associated with image processing to determine the geometric characteristics of the drop. This paper presents the results on the dynamics of methanol drops during evaporation. These results are obtained using an experimental setup where the operating conditions are well controlled by the adequate instrumentation and the behavior of the methanol drop during its evaporation is followed using two cameras from top and side views.

In the following, we first present the experimental setup and the associated instrumentation to control the operating conditions and the method to determine the geometric characteristics of the drop. The next section is devoted to the presentation of the results obtained in the form of images and graphical representations followed by discussion and qualitative interpretation. We will end up with a conclusion that summarizes the main results.

2. Materials and methods

The experimental setup has been designed and realized to follow and characterize the evolution of the drop shape during its evaporation. The schematic of the test cell with its instrumentation is represented in Fig. 1.

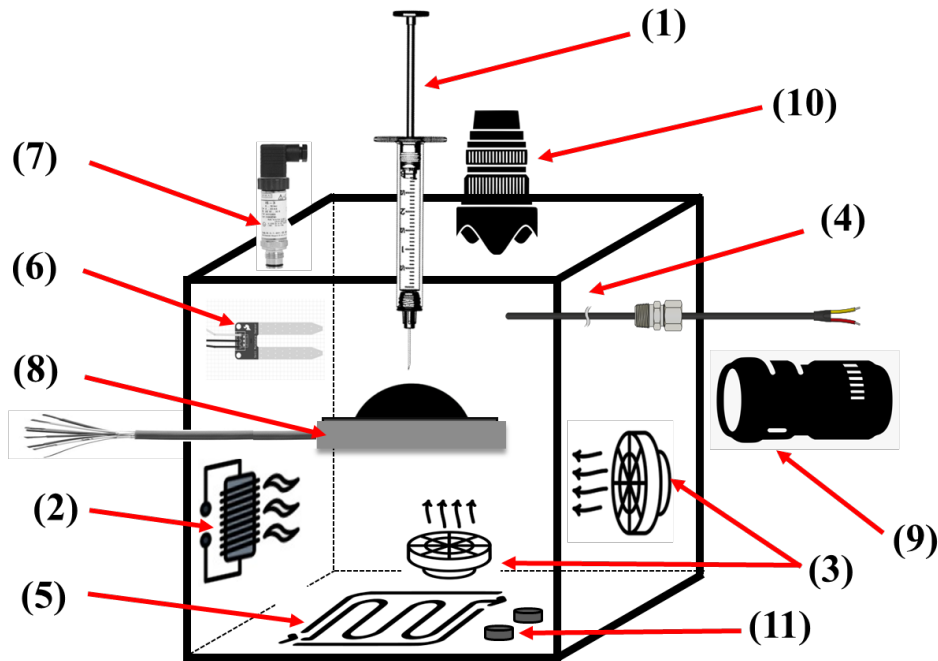


Fig. 1. Schematic view of the cell and its main components for the control of the surrounding environment and boundary conditions:
 (1) syringe, (2) heating resistors, (3) fans, (4) thermocouple, (5) heat exchanger, (6) hygrometer, (7) pressure sensor, (8) heat flux sensor, (9) side view camera, (10) top view camera, (11) evaporator

The cubic cell of 11.5 cm side is designed in such a way to isolate the droplet from the external environment perturbations like natural convection, external humidity and to control accurately the working conditions (temperature, pressure, relative humidity and substrate temperature). The drop is deposited using a micro-syringe (1) which is mounted on an injection system that allows to accurately control the volume of the drop. Inside the cell, the temperature is controlled by two heating resistors (2) equipped with a rheostat and regulators, a heat exchanger (5) and two fans (3) and it is measured by thermocouple (4). Whereas, the humidity is controlled by an evaporator (11) and measured with a humidity sensor (6) placed inside the cell. The controlled pressure is measured using a piezoelectric pressure sensor (7). A heat flux sensor (8) is used to evaluate heat transfer rate between the substrate and the droplet. The apparatus is instrumented with two cameras (9) and (10) in order to record the droplet shape evolution from the side view and the top view to observe the drop behavior during the

evaporation and determine the geometric parameters (contact angle, contact line diameter and wetting surface area) by an image processing tool.

3. Experimental procedure and image analysis

3.1. Experimental procedure

The experiments performed in this study start with the substrate preparation followed by the droplet injection. A 100 μm thin sheet of aluminum foil is used as a substrate. The operating conditions (temperature, relative humidity, ...) are tuned and controlled continuously and the measurements (temperature, drop shape, ...) are conducted during the evaporation process. At the end, the recorded data are processed.

After closing the cell, the operating conditions are adjusted using programmable temperature controllers (PID-type), the resistors, the heat exchanger, the dehumidification system and the evaporator. Thus, the operating conditions are set at a temperature $T = 25^\circ\text{C}$, a relative humidity of water in the air $H_r = 40\%$ and a total pressure $P = 1 \text{ atm}$ with an uncertainty of $\pm 0.5^\circ\text{C}$ for the temperature of the cell, $\pm 0.2^\circ\text{C}$ for the temperature of the substrate, $\pm 2\%$ for the relative humidity and $\pm 10^{-2} \text{ atm}$ for the total pressure. All these conditions are maintained during the evaporation period. The relative humidity of methanol in the air is initially at 0% and 0.3% at the total evaporation.

We controlled and maintained constant the temperatures of the cell and that of the substrate separately. Firstly, for the control of the cell temperature, we have used a heat exchanger and two electric resistors. The heat exchanger is connected to a thermoregulation system from the Lauda® ECO E10 series. The resistors are utilized for the temperature control using PID regulators linked to the thermocouple (4) close to the droplet (Fig. 1). Secondly, for the substrate temperature control, we have used the thermocouple inserted in the heat flux sensor, which is stuck by a thermal grease to the substrate. This thermocouple is controlled with

a PID and kept at a desired level by the electrical power supply. Figure 2 shows an example of the recorded temperatures of the cell and the substrate during the experiments.

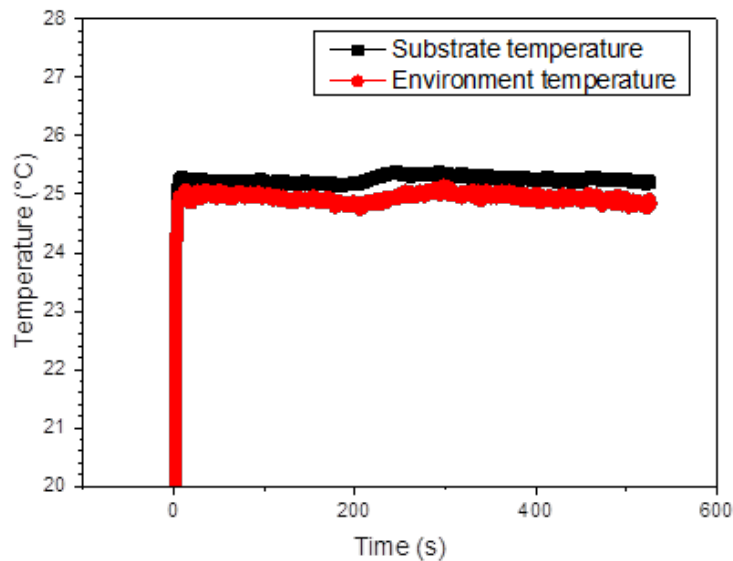


Fig. 2. Environment and substrate temperature evolution during experiments. initial volume = 8.4 μL , temperature of the cell and substrate = 25°C, liquid temperature = 25°C, relative humidity air-water = 40%, relative humidity of methanol in the air = 0%, pressure = 1 atm.

After filling the micro-syringe with the testing liquid (methanol), it is placed in the injection system and the liquid is deposited on the substrate to generate a sessile drop. At the moment when the drop enters in contact with the substrate, the needle must remain immersed in the drop and the injection must be done at a constant flowrate. When the desired volume is reached, the needle is removed. Immediately after the injection of the droplet on the substrate, two systematic checks are carried out: the first on the injected volume and the second on the shape and wettability of the drop, in order to decide on the validity of the recording and on its exploitation. For each test, two cameras record the shape of the droplet from two views: the camera (9) from the front side and the camera (10) from the top side.

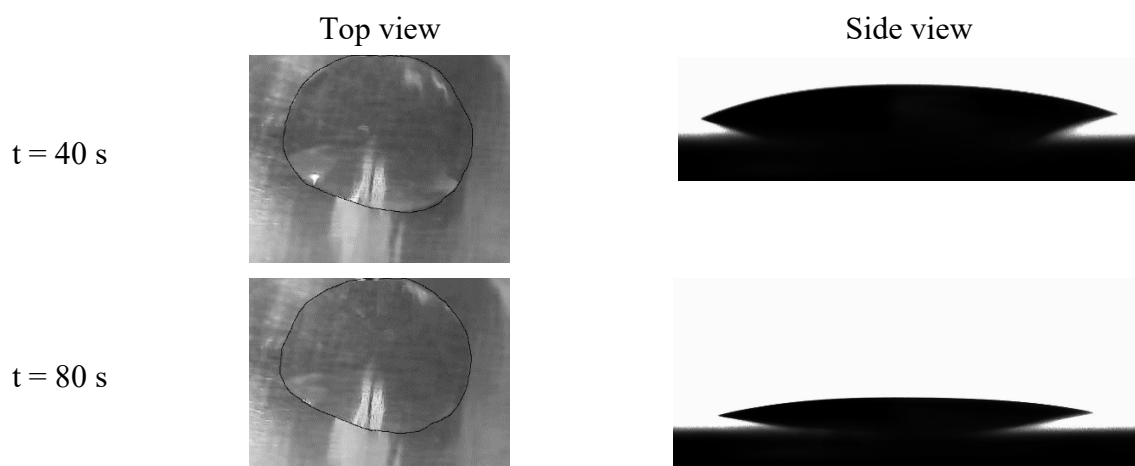
3.2. Image analysis

The two cameras are adjusted to take 30 frames/second and a resolution of 1600 x 1200 pixels in order to reduce the size of the recorded video and the memory unit. Several

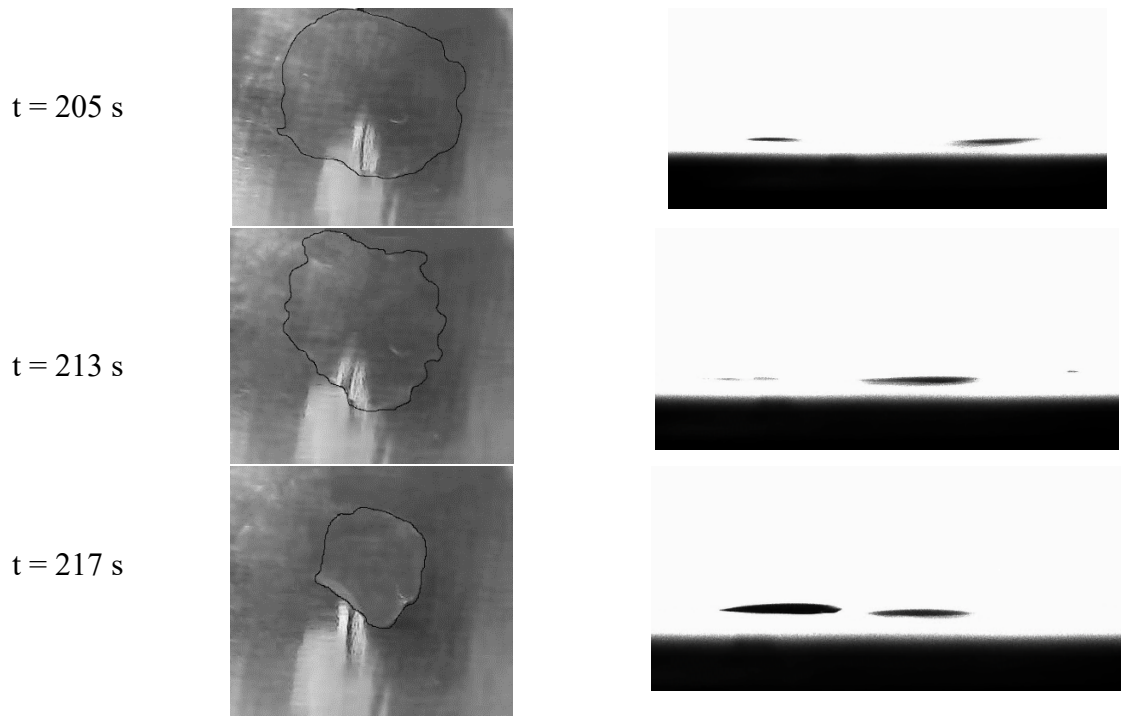
adjustments are necessary to make a good picture. The accuracy of these settings determines the technical quality of the image, especially its sharpness and exposition.

Once the drop has completely evaporated, the recordings are stopped and the data processing is started. The recorded video of the sessile drop is processed by sequencing it into images then the treatment is done using IC MEASURE software which provides a very broad range of applicability with respect to different image types and quality and a drop shape analysis software established from two methods namely Drop Snake which is based on B-spline snakes (active contours) to shape the drop and LBADSA which is based on the fitting of the Young-Laplace equation to the image data [29-30].

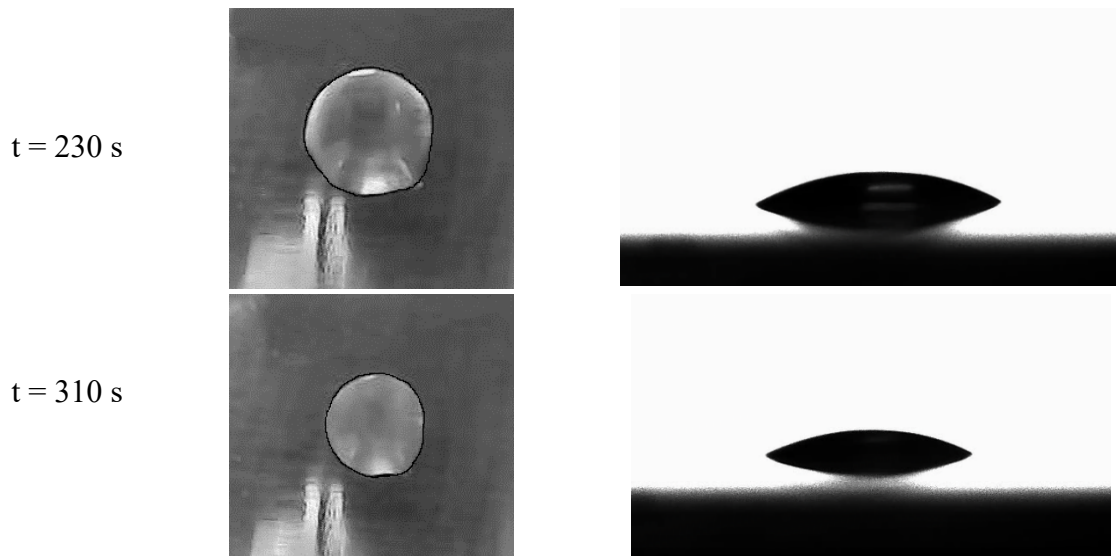
During the evaporation process, three distinct stages are highlighted. In the following paragraph, each stage is described with the associated image processing to determine the geometric properties of the drop (contact line diameter, wetting surface area and contact angle); the volume is then computed from geometric parameters as described later. We note that experiments were performed for three different droplet volumes, 1 μL , 5 μL and 8.4 μL , with an uncertainty of $\pm 0.1 \mu\text{L}$.



(a) Top and side views of the drop shape in the first stage



(b) Top and side views of the drop shape in the second stage



(c) Top and side views of the drop shape in the third stage

Fig. 3. Drop shape from top and side views. Initial volume = $8.4 \mu\text{L}$, temperature of the cell and substrate = 25°C , liquid temperature = 25°C , relative humidity air-water = 40% , relative humidity of methanol in the air = 0% , pressure = 1atm .

Figure 3 (a, b and c) displays the drop shape from the top and side views for the different stages observed during the evaporation. In the first stage (Fig. 3(a)), the droplet has a quasi-axisymmetric shape and it evaporates in a “nearly pinned mode” with a very slight shrinkage

of the contact line and a decreasing contact angle. At a limit contact angle of 3.4° , the end of the first stage, the droplet starts to destabilize. Fig. 3(b) shows a front and top view at different instants of the second stage. In this stage, the contact line deforms with very important dynamics. First, the occurrence of interface undulations is observed, then a flattening of the droplet to form a very thin liquid film and the occurrence of the contact line deformations. The wetting drop area evolves from its quasi-circular shape to a perturbed shape. It is worth noting that this observation would not have been possible without the top view camera (10). The front camera (9) alone allows to see partially the droplet. The fluctuating movements of the contact line and the interface of the droplet lead to a fluctuating behavior of the droplet in a front view.

After this second stage characterized by fluctuations of the interface and contact line, the evaporating droplet shrinks and takes a spherical cap shape with a “quasi-circular” contact line. Figure 3(c) displays the droplet in top and front views during the third stage where the evaporation continues with slower kinetics than in stages 1 and 2.

In most studies of sessile droplets, the assumption of axisymmetry is applied for the computation of the drop volume because the observations are made only from the side view. In the case of methanol this approach gives incorrect results because the axisymmetric shape of the drop is lost because of 3D effects. The use of the top view allowed to observe the dynamics of methanol evaporation especially in the second stage which is accompanied by the contact line motion.

For hemispherical sessile drops, the volume can be expressed geometrically as a function of only two parameters: the contact angle and the base radius according to the following formula:

$$V(R, \theta) = \frac{\pi R^3}{3} \frac{(1 - \cos \theta)^2 (2 + \cos \theta)}{\sin^3 \theta} \quad (1)$$

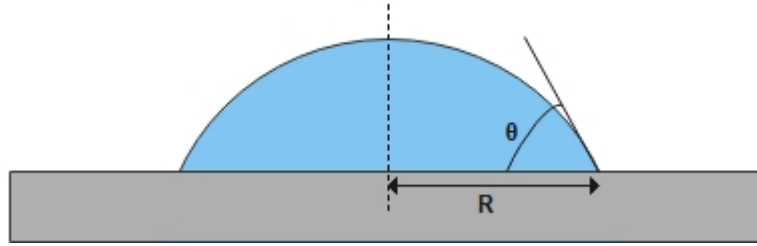


Fig. 4. Schematic of the sessile droplet with R being the averaged value of the base radius obtained from the top view and θ the contact angle obtained from the side view.

Because of the loss of symmetry of the drop shape, the contact line diameter measured by the front camera is not correct. Therefore, we followed another approach based on the computation of the equivalent diameter based on the wetting surface area of the drop in contact with the substrate. This equivalent diameter is deduced from the wetting area of the drop measured with the top camera without making any simplifying assumption about the shape of the droplet. The wetting surface area is computed using a refined meshing in order to have a good accuracy. For the sake of brevity, we do not detail the numerical technique in the present study.

The contact angle is measured from images with the side view camera. This value is assumed to be the same for all directions in stages 1 and 3 where the contact line keeps its circular shape. In the second stage, the contact line varies in time, we cannot obtain values of the contact angle for the second stage by the drop shape analysis software mentioned above. Therefore, we proceeded manually to get an average contact angle at given instant within a very short time period. The procedure will be detailed later.

4. Experimental results

In this section, we present the evolution of the wetting surface area, the contact angle and the volume of the drop during all the evaporation period i.e. the three observed stages. The first stage with a fast evaporation kinetics, followed by a second stage characterized by a fluctuating motion of the drop and then the third stage with a slower evaporation kinetics.

4.1. Wetting surface area and contact line diameter

The camera located above the drop allows tracking the droplet shape from the top view during the entire evaporation stages. The image-by-image analysis allows to obtain the variation of the wetting surface area.

Figure 5 shows the variations of the wetting area of the drop with the substrate. As we can see, three different behaviors are observed. In a first period, the surface contact area decreases very slightly during the drop evaporation. In the second stage, the contact line starts to show different patterns depending on the location. In this stage, the contact line retracts more strongly in some places than others with disturbed shapes. It exhibits sawtooth deformations which evolve in time. These deformations in space are of small magnitude and wavelength (Fig. 3b, time = 231s). Thus, the wetting area of the drop decreases sharply to a given value. In the third stage, the variation of the wetting area decreases slightly until the end of the drop evaporation. In this stage the contact line becomes smooth again with a quasi-circular shape.

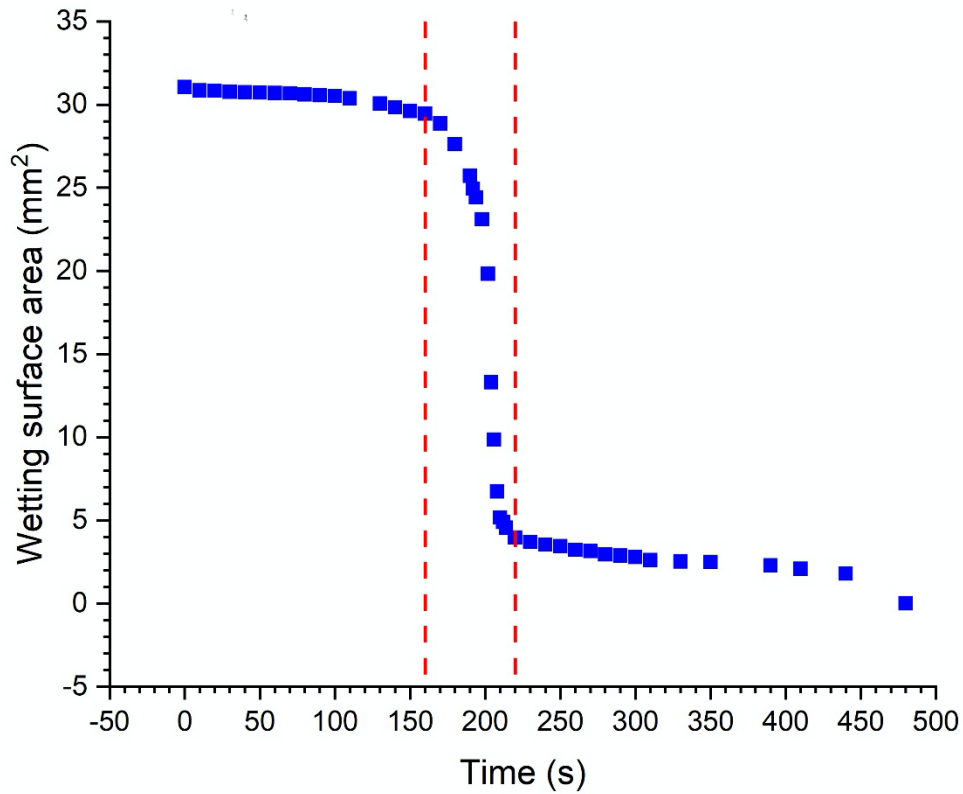


Fig. 5. Variation of the wetting surface area of the droplet with the substrate as a function of time: initial volume = 8.4 μL , temperature of the cell and substrate = 25°C, liquid temperature = 25°C, relative humidity air-water = 40%, relative humidity of methanol in the air = 0%, pressure = 1 atm.

The limits of each stage are determined from Fig.5 by the substantial change in the slope of the wetting surface curve. To better understand the behavior of the contact line during the evaporation process, the variation of the contact line diameter as a function of time is plotted in Fig.6, using the top and side views. The same trend as the wetting surface is exhibited. We recall that the contact diameter from the top view is a mean value computed from the measurement of the wetting surface using image analysis. Whereas, the diameter from the side view is a value obtained directly with IC MEASURE software. With the top view camera (blue symbols in Fig.6), we observe a very slow decrease of the contact diameter in the first stage followed at the end by a sharp decline that corresponds to the start of the second stage. During this stage, the diameter decreases abruptly corresponding to the behavior of the wetting surface

as described previously in Fig.5. In the third stage, the contact diameter evolves with a very slow evaporation rate. However, with the side view camera (red symbols in Fig.6), the contact diameter decreases with a different law in the first stage compared to the top view results. In the second stage, the contact diameter is difficult to measure because of the 3D effects that are clearly shown with the top view camera. Therefore, the side view measurements give erroneous values for the contact diameter (Fig 6). In the third stage, the top and side views give similar contact diameter which indicates that the drop recover its axisymmetric shape.

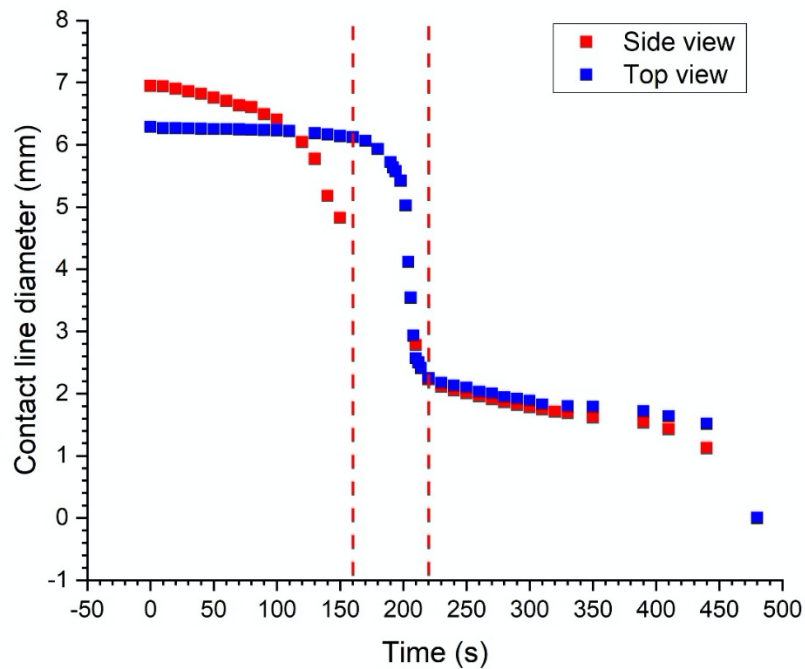


Fig. 6. Variation of the contact line diameter of the droplet with the substrate as a function of time: initial volume = $8.4 \mu\text{L}$, temperature of the cell and substrate = 25°C , liquid temperature = 25°C , relative humidity air-water = 40% , relative humidity of methanol in the air = 0% , pressure = 1atm .

As a result, the image analysis of the evaporation of sessile drop proves the weakness of the use of the side camera alone. It requires a second camera from the top view for a more accurate analysis.

4.2. Contact angle

The contact angle is linked to the interfacial tensions involved and its determination enables the wettability of the surface studied by the liquid being tested. Therefore, the contact angle measurement allows to characterize the adhesion between the liquid and the substrate.

For the first and the third stage, we have used a drop shape analysis method [22] which allows the calculation of contact angles from sessile drop images. For the second stage the contact angle is more difficult to measure due to the behavior of the droplet which is associated with surface and contact line motions. In our case, we have proceeded according to the method mentioned in section 3.2. In fact, as the wetting area evolves in time, the contact angle changes. Therefore, we determined the contact angle at a fixed time by averaging the measured contact angle over a short period of time ($<1s$). In Fig.7, the contact angles shown in the second stage correspond to the mean contact angle at each fixed time. The bars correspond to the maximum and minimum values in this period.

It can be seen that the contact angle values decrease linearly in time until the end of the first stage. When the wetting surface starts to shrink (second stage), the use of the software is no longer possible, the estimation of the contact angle gives sharply increasing values towards higher values than the initial ones at the beginning of the evaporation. Later, at the third stage, when the smaller droplet is formed, we can use again of the drop shape analysis software. This last stage is characterized by a continuous decrease of the contact angle until the end of the evaporation. The open triangles are obtained by interpolation in order to compute the drop volume in this period of time where the contact angle is not measurable because of the small size of the drop.

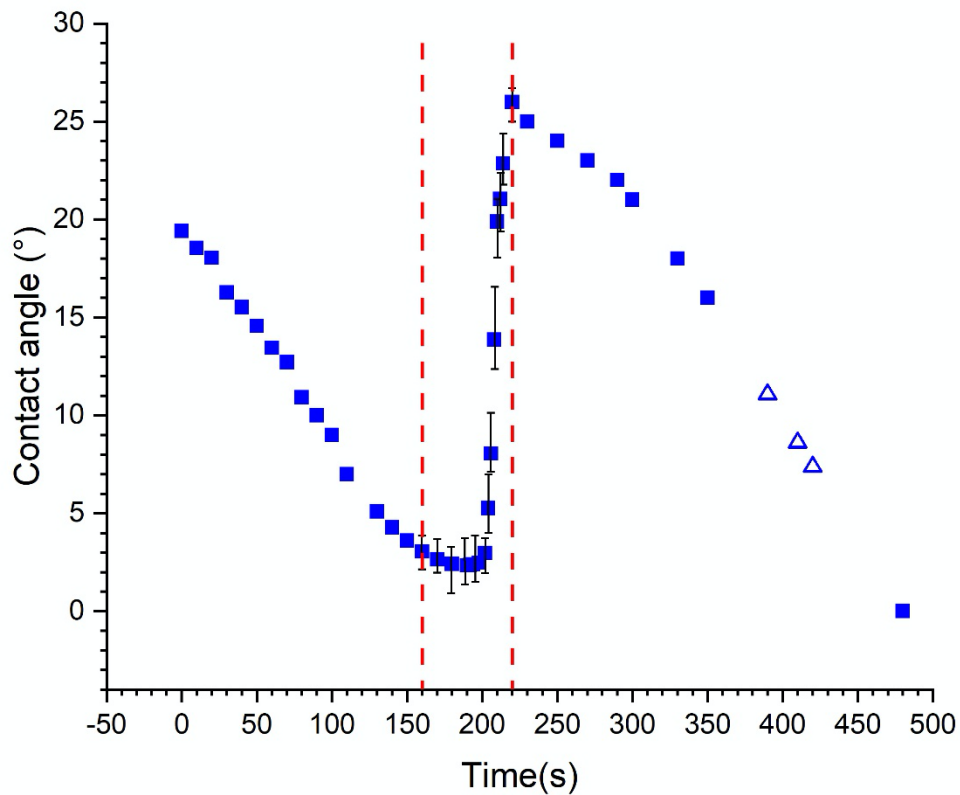


Fig. 7. Variation of the contact angle of the droplet with the substrate as a function of time: initial volume = $8.4 \mu\text{L}$, temperature of the cell and substrate = 25°C , liquid temperature = 25°C , relative humidity air-water = 40% , relative humidity of methanol in the air = 0% , pressure = 1 atm . The solid square symbols are the measured values. The open triangles are the interpolated values

4.3. Drop volume

In order to have a better understanding of the evaporation kinetics of the methanol droplets we need to go through the computation of the volume during the evaporation by following the previously mentioned approach which combines the measurement of the contact angle from images with the side camera and the equivalent radius of a circle of the same wetting area measured with the top camera.

In the second stage the drop volume is computed using the contact angle value as described previously in subsection 4.2. Figure 8 shows the evolution of the evaporation kinetics

over the entire evaporation period. In stages 1 and 3 the evaporation rates are constant but differ significantly. It is equal to $0.0486 \mu\text{L/s}$ in the first stage 1 and $0.0018 \mu\text{L/s}$ in the third stage 3. In the second stage the drop volume transits from the two values continuously over a short time.

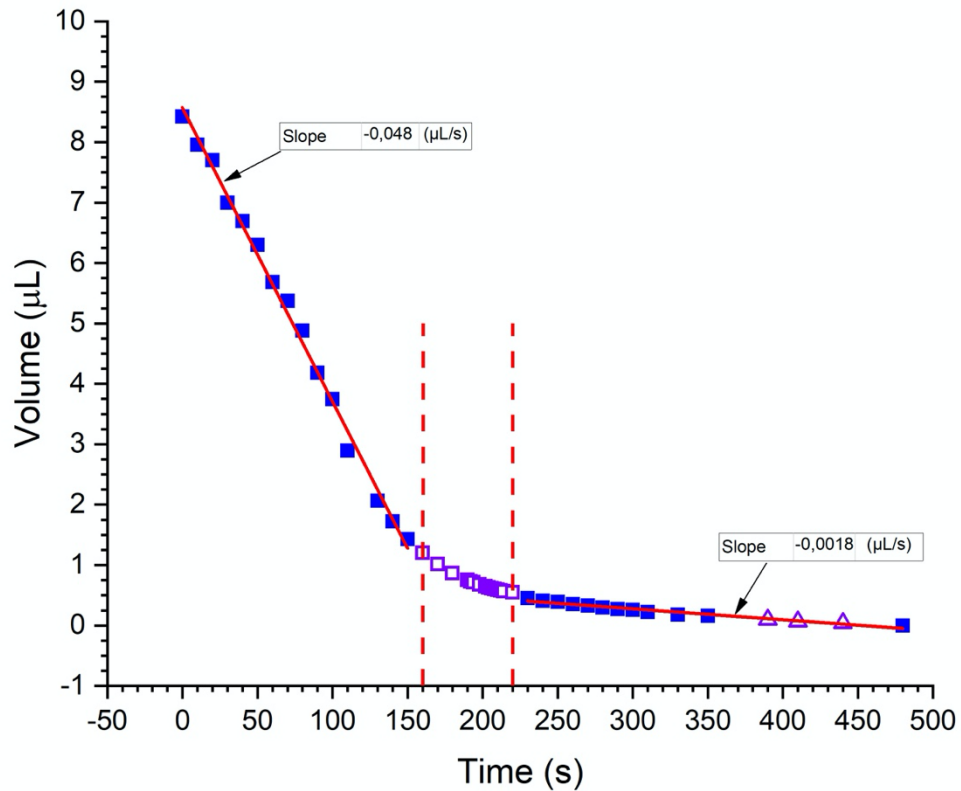


Fig. 8. Variation of the volume of the droplet as a function of time using estimated contact angle measurements: initial volume = $8.4 \mu\text{L}$, temperature of the cell and substrate = 25°C , liquid temperature = 25°C , relative humidity air-water = 40% , relative humidity of methanol in the air = 0% , pressure = 1atm . The solid square symbols are the measured values. The open squares are calculated with the mean contact angles in the second stage. The open triangles are the computed values corresponding to the interpolated contact angle

The evaporation duration of stages 1 and 3 are much longer than the second stage, which corresponds to a transition regime that takes place in a disordered way, probably in connection with the local mechanical conditions of the droplet. The contact line retracts until it reaches a new wetting angle. In the third stage, the droplet has again an almost circular contact line but much smaller than in the first evaporation stage.

4.4. Influence of the initial drop volume

In order to investigate the behavior of the methanol droplet during evaporation for other drop volumes additional experiments are conducted. Figure 9 shows the evolution of the non-dimensional wetting surface area $S^* = \frac{S}{S_i}$ as a function of the non-dimensional time $t^* = \frac{t}{t_f}$. The time is scaled with the droplet lifetime t_f and the wetting surface scaled with the initial wetting area S_i . As we can see, the laws of variation in this system of coordinates are well superimposed with, however, a slight shift between the curve of 8.4 μl and the curves of 1 and 5 μl . In all three cases we observe a small decrease of the wetting surface area in the first stage, then a sharp decline in the second stage and finally a very slow decrease of the wetting area in the third stage. We can also notice that the transition lines occur at the same time ($S_{12}^* = 0,91 - t_{12}^* = 0,33; S_{23}^* = 0,15 - t_{23}^* = 0,45$).

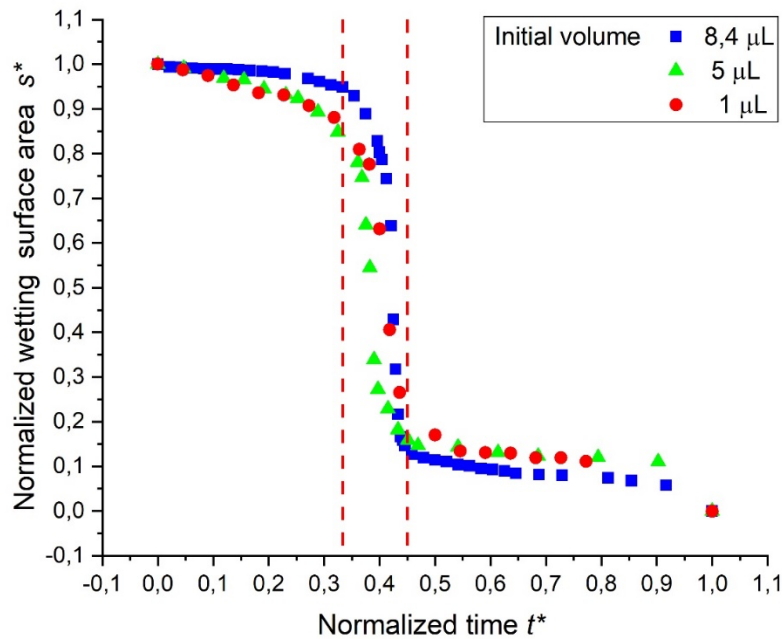


Fig. 9. Variation of the normalized wetting surface area of the droplet with the substrate as a function of normalized time: initial volume = 8.4 μL , 5 μL and 1 μL , temperature of the cell and substrate = 25°C, liquid temperature = 25°C, relative humidity air-water = 40%, relative humidity of methanol in the air = 0%, pressure = 1atm.

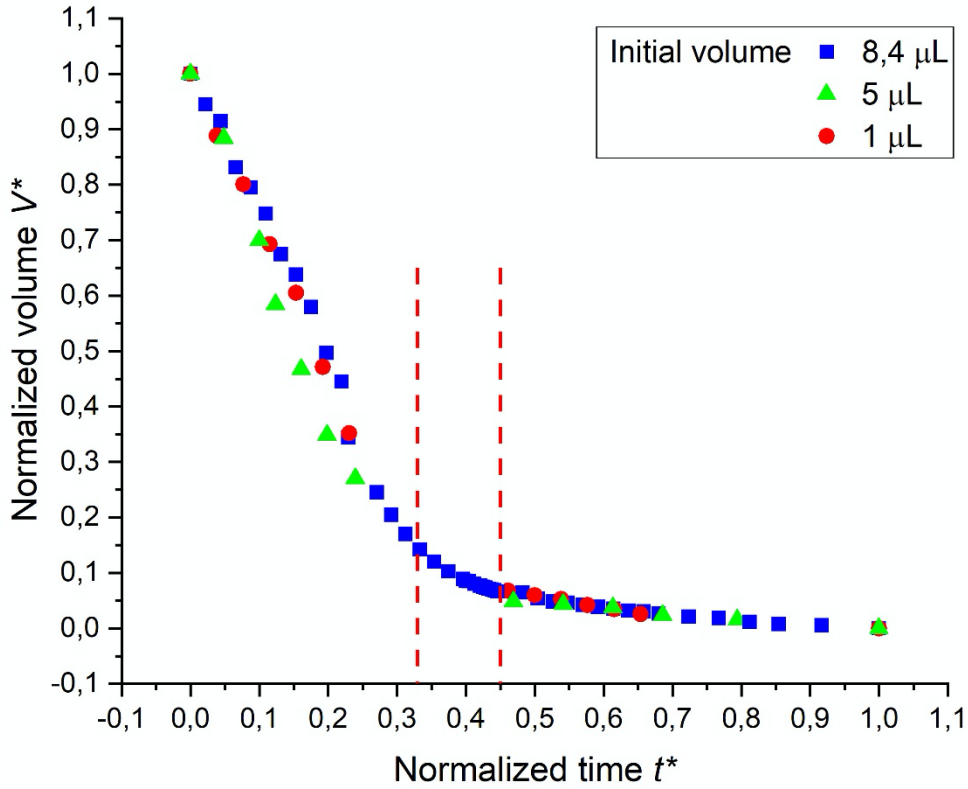


Fig. 10. Variation of the normalized volume of the droplet as a function of normalized time: initial volume = 8.4 μL , 5 μL and 1 μL , temperature of the cell and substrate = 25°C, liquid temperature = 25°C, relative humidity air-water = 40%, relative humidity of methanol in the air = 0%, pressure = 1 atm.

Figure 10 shows the evolution of the drop volume $V^* = \frac{V}{V_i}$ as a function of the time $t^* = \frac{t}{t_f}$ in non-dimensional coordinates. The volume V is scaled with the initial drop volume V_i . The variation laws of the drop volumes in these coordinates coincide very well for the three drop volumes studied. We clearly identify the three stages. We observe a strong decrease of the volume of the drop in the first stage according to a "linear" law. In the third stage this decrease is also linear with a slope much lower than that of the first stage of evaporation. In the second stage the volume of the drop varies continuously from the end of the first stage to the beginning of the third stage. The second stage corresponds to the following coordinates ($V_{12}^* = 0,15 - t_{12}^* = 0,33$; $V_{23}^* = 0,08 - t_{23}^* = 0,45$).

As we can see, the three stages show the same behavior whatever is the initial drop volume. These results prove the robustness of the phenomena observed in the case of methanol evaporation.

5. Conclusion

We realized a new experimental setup to study the evaporation of sessile droplets under well controlled environmental conditions. We have also implemented an instrumentation to follow the variations of the geometrical characteristics of sessile droplets during their evaporation. This instrumentation allowed to determine the geometric parameters of the methanol droplet using image analysis.

This approach gave us the opportunity to highlight an original behavior of the evaporation of a methanol droplet in moist air. It is characterized by three distinct stages with different evaporation kinetics. In particular, we have highlighted a transition stage characterized by a sharp decrease in the wetting surface area with a contact line in sawtooth shape. We have shown the robustness of the phenomenon which was similar for three droplet volumes studied (1 μl , 5 μl and 8.4 μl).

This work will be continued with a detailed analysis of the phenomena revealed for the evaporation of high volatility liquid. These results will be compared to the case of low volatility fluids such as water.

References

- [1] M. F. B. Stodt, J. Kiefer, U. Fritsching, Ethanol droplet formation: dynamics and combustion mode in the flame of the SpraySyn-nozzle, *Experiments in Fluids* 60 (8) (2019) 125. <https://doi.org/10.1007/s00348-019-2771-9>
- [2] W. Deng, A. Gomez, Electrospray cooling for microelectronics, *Int. J. Heat and Mass Transfer* 54 (11) (2011) 2270-2275. <https://doi.org/10.1016/j.ijheatmasstransfer.2011.02.038>

- [3] E. Sowade, T. Blaudeck, R. R. Baumann, Self-Assembly of Spherical Colloidal Photonic Crystals inside Inkjet-Printed Droplets, *Crystal Growth & Design* 16 (2) (2016) 1017-1026. <https://doi.org/10.1021/acs.cgd.5b01567>
- [4] G. Ciasca, L. Businaro, M. Papi, A. Notargiacomo, M. Chiarpotto, A. De Ninno, V. Palmieri, S. Carta, E. Giovine, A. Gerardino, M. De Spirito, Self-assembling of large ordered DNA arrays using superhydrophobic patterned surfaces, *Nanotechnology* 24 (49) (2013) 495302. <https://doi.org/10.1088/0957-4484/24/49/495302>
- [5] R. Blossey, Self-cleaning surfaces, virtual realities, *Nature Materials* 2 (5) (2003) 301-306. <https://doi.org/10.1038/nmat856>
- [6] D. J. Norris, E. G. Arlinghaus, L. Meng, R. Henry, L. E. Scriven, Opaline Photonic Crystals: How Does Self-Assembly Work?, *Advanced Materials* 16 (16) (2004) 1393-1399. <https://doi.org/10.1002/adma.200400455>
- [7] B. Sobac, D. Brutin, Structural and evaporative evolutions in desiccating sessile drops of blood, *Phys. Rev. E*. 84(1) (2011) 011603. <https://doi.org/10.1103/PhysRevE.84.011603>
- [8] T. Young, An essay on the cohesion of fluids, *Phil. Trans. R. Soc. Lond.* 95 (1805) 65–87. <https://doi.org/10.1098/rstl.1805.0005>
- [9] P.S. Laplace, *Théorie de l'action capillaire—Supplément au dixième livre du traité de mécanique céleste*, Courcier, Paris, 1806.
- [10] H. Y. Erbil, Evaporation of pure liquid sessile and spherical suspended drops: A review, *Advances in Colloid and Interface Science* 170 (1–2) (2012) 67-86. <https://doi.org/10.1016/j.cis.2011.12.006>
- [11] H. Y. Erbil, Dependency of Contact Angles on Three-Phase Contact Line: A Review, *Colloids and Interfaces* 5(1) (2021) 8. <https://doi.org/10.3390/colloids5010008>

- [12] S. Chatterjee, M. Kumar, J. S. Murallidharan, R. Bhardwaj, A review on the evaporation of sessile droplets on solid surfaces under different experimental conditions, *Advances in Multiphase Flows*, 1st Ed., Chap. 1, Begell House Publishers, Jan. 2022
- [13] M. Gao, P. Kong, L. Zhang, Evaporation dynamics of different sizes sessile droplets on hydrophilic and hydrophobic heating surface under constant wall heat fluxes conditions, *Int. Comm. Heat and Mass Transfer* 93 (2018) 93-99.
<https://doi.org/10.1016/j.icheatmasstransfer.2018.03.007>
- [14] M. Ait Saada, S. Chikh, L. Tadrist, A numerical study of particle transport in an evaporating colloidal sessile droplet, *Interf. Phen. Heat Transfer* 4 (4) (2016) 217-233.
<https://doi.org/10.1615/InterfacPhenomHeatTransfer.2017019419>
- [15] A. Marmur, C. Della Volpe, S. Siboni, A. Amirfazli, J. W. Drelich, Contact angles and wettability: towards common and accurate terminology, *Surface Innovations* 5(1) (2017) 3-8.
<https://doi.org/10.1680/jsuin.17.00002>
- [16] G. V. Kuznetsov, P. A. Strizhak, R. S. Volkov, Heat exchange of an evaporating water droplet in a high-temperature environment, *Int. J. Therm. Sc.* 150 (2020) 106227.
<https://doi.org/10.1016/j.ijthermalsci.2019.106227>
- [17] Y. Lin, F. Chu, X. Wu, Evaporation and boiling of water-alcohol droplets: Dynamic characteristics of wetting and heat transfer, *Int. Comm. Heat and Mass Transfer* 134 (2022) 106045. <https://doi.org/10.1016/j.icheatmasstransfer.2022.106045>
- [18] K. Sefiane, L. Tadrist, Experimental investigation of the de-pinning phenomenon on rough surfaces of volatile drops, *Int. Comm. Heat and Mass Transfer* 33 (4) (2006) 482-490.
<https://doi.org/10.1016/j.icheatmasstransfer.2005.12.010>
- [19] S. Ye, L. Zhang, C. M. Wu, Y. R. Li, Q-S. Liu, Experimental investigation on evaporation dynamics of sessile ethanol droplets on a heated substrate, *Int. J. Heat and Mass Transfer* 162 (2020) 120352. <https://doi.org/10.1016/j.ijheatmasstransfer.2020.120352>.

- [20] A. Maatar, S. Chikh, M. Ait Saada, L. Tadrist, Transient effects on sessile droplet evaporation of volatile liquids, *Int. J. Heat and Mass Transfer* 86 (2015) 212-220, <https://doi.org/10.1016/j.ijheatmasstransfer.2015.02.077>.
- [21] T. M Chang, L. X Dang, Liquid–vapor interface of methanol–water mixtures : a molecular dynamics study, *The Journal of Physical Chemistry B* 109 (12) (2005) 5759-5765, <https://doi.org/10.1021/jp045649v>
- [22] C. K Chiang, Y. W Lu, Evaporation phase change processes of water/methanol mixtures on superhydrophobic nanostructured surfaces, *Journal of Micromechanics and Microengineering* 21(7) (2011) 075003, <https://doi.org/10.1088/0960-1317/21/7/075003>
- [23] R. J Hopkins, J. P Reid, A comparative study of the mass and heat transfer dynamics of evaporating ethanol/water, methanol/water, and 1-propanol/water aerosol droplets, *The Journal of Physical Chemistry B* 110 (7) (2006) 3239-49, <https://doi.org/10.1021/jp056523g>
- [24] L. Bin, R. Bennacer, A. Bouvet, Evaporation of methanol droplet on the Teflon surface under different air velocities, *Appl. Therm. Eng.* 31 (2012) 3792–3798, <https://doi.org/10.1016/j.applthermaleng.2011.07.018>
- [25] S. Andalib, S. Alshehri, A. Kavehpour, P. Combined effect of relative humidity and substrate temperature on evaporation of methanol droplet, *Journal of Coatings Technology and Research* 16 (6) (2019) 1691-1698, <https://doi.org/10.1007/s11998-019-00271-w>
- [26] B. Liu, B. Cai, Y. Su, X. Dong, A theoretical and experimental study of the evaporation rate of methanol droplets on a horizontal surface, *Int. J. Air-Cond.* 21 (03) (2013) 1350019. <https://doi.org/10.1142/S2010132513500193>.
- [27] T. S Wang, W. Y Shi, Transition of Marangoni convection instability patterns during evaporation of sessile droplet at constant contact line mode, *Int. J. Heat and Mass Transfer* 148 (2020) 119138, <https://doi.org/10.1016/j.ijheatmasstransfer.2019.119138>

[28] T. S Wang, W. Y Shi, Influence of substrate temperature on Marangoni convection instabilities in a sessile droplet evaporating at constant contact line mode, *Int. J. Heat and Mass Transfer* 131 (2019) 1270-1278, <https://doi.org/10.1016/j.ijheatmasstransfer.2018.11.155>

[29] A. F. Stalder, G. Kulik, D. Sage, L. Barbieri, P. Hoffmann, A snake-based approach to accurate determination of both contact points and contact angles, *Colloids and Surfaces A: Physicochemical and Engineering Aspects* 286 (1) (2006) 92-103.

<https://doi.org/10.1016/j.colsurfa.2006.03.008>

[30] A. F. Stalder, T. Melchior, M. Müller, D. Sage, T. Blu, M. Unser, Low-bond axisymmetric drop shape analysis for surface tension and contact angle measurements of sessile drops, *Colloids and Surfaces A: Physicochemical and Engineering Aspects* 364 (1) (2010) 72-81.

<https://doi.org/10.1016/j.colsurfa.2010.04.040>